JP2.6 LIGHT RAIN RETRIEVALS USING CLOUDSAT 94-GHZ RADAR DATA - PRELIMINARY RESULTS

Cristian Mitrescu[1*] John M. Haynes[2] Tristan L'Ecuyer[2] Steven D. Miller[1] Joe Turk[1]

[1]Naval Research Laboratory, Marine Meteorology Division, Monterey, CA.
[2]Department of Atmospheric Science, Colorado State University, Fort Collins, CO.

1. INTRODUCTION

Clouds play a crucial role in the climate system through a myriad of non-linear feedback processes (Held and Soden, 2000). Precipitation generated by a subset of these clouds is a central component of the Earth's hydrological cycle with far-reaching impacts to the planet's energy balance and sustenance of its living inhabitants. In gauging subtle changes to the climate system in response to anthropogenic forcing, for example, it is therefore of high relevance to hold a detailed and thorough understanding of the global precipitation field. Given the three-dimensional structure of rainfall, measuring its distribution and intensity is a problem perhaps best suited to an active sensor that is capable of penetrating and range-resolution the entire atmospheric volume.

The first spaceborne radar applied to quantitative precipitation estimation (QPE) was demonstrated on the highly successful Tropical Rainfall Measuring Mission (TRMM), a satellite dedicated as its name implies to and characterizing the distribution of rainfall in the tropics. Given its specific mission, the TRMM Precipitation Radar (PR) was not designed to sense light rainfall (e.g., rainrates less than about 1 mm/hr), and its low-inclination orbit omits cover of mid-to-upper latitudes where such light rain (and snowfall) is most common. From a global climate perspective, however, this light rain component (particularly the fraction occurring over land surfaces) cannot be ignored. In 2006, NASA's Earth System Science Pathfinder Project (ESSP) launched the CloudSat (Stephens et al., 2002) and CALIPSO satellites; the latest in a series of small, low-cost, rapid turn-around exploratory earth science missions. While CALIPSO is geared toward measurement of aerosol studies and aerosol indirect effects (which have potentially significant ramifications to light rainfall in their own right) by way of a 532 nm lidar, the CloudSat 94-GHz (3 mm wavelength) Cloud Profiling Radar (CPR) has the capability to sense not only the vertical microphysical structure of clouds but also the any light-to-moderate (i.e., 1.0 mm/hr to perhaps 5-10 mm/hr) rainfall and drizzle ($<$ 1.0 mm/hr) component that currently goes undetected by the TRMM/PR.

This paper provides an update on progress to exploit the light rainfall detection capability of CloudSat. In light of the multiple challenges (both algorithms and sensor hardware) associated with harnessing the potential of this new sensor dataset, the results presented at this very early stage in the retrieval development are regarded as very preliminary and subject to change. As such, this paper will focus primarily on the observing system itself and the methodology used to extract rainfall from measurements of raw power return.

*Corresponding author address: Cristian Mitrescu, Naval Research Laboratory, 7 Grace Hopper Ave. MS#2, Monterey, CA 93943-5502; e-mail: cristian.mitrescu@nrlmry.navy.mil.

2. THE CLOUDSAT OBSERVING SYSTEM: THE 94-GHZ RADAR

Launched in the early morning hours of April 28-th 2006 from Vandenberg Air Force Base in California, the CloudSat radar and CALIPSO lidar joined the so-called "A-Train" satellite constellation (led by EOS-Aqua). These two novel active sensors were chartered to clouds, aerosol, and their links to climate change on many temporal and spatial scales. The CPR has a vertical resolution of 240 m and a footprint of roughly 1.4 (cross track) $\times 2.3$ (along-track) km. Having a sensitivity around -32 dBZ, due to time-averaging over a 0.16 sec interval, the CPR can effectively profile a wide variety of cloud types ranging from fair weather cumulus to the most intense tropical systems, including their precipitating signature (within the limits of attenuation). It however misses tenuous cirrus clouds, due to their overall very low backscatter returns, and has demonstrated some difficulties in resolving boundary layer cloudiness due to surface clutter effects. CloudSat follows immediately behind Aqua, which carries a suite of passive sensors such as AIRS/AMSU-A/HSB, AMSR-E, CERES and MODIS ($http://aqua.nasa.gov$). The CALIPSO lidar, trailing closely behind CloudSat, is most sensitive to thin high level cirrus, aerosols, and boundary layer structures, but rapidly attenuates most optically thick cloud systems. The right ascension of the CloudSat and CALIPSO ascending nodes are displaced roughly 5 degrees east of Aqua in order to avoid specular reflection off the ocean surface (sunglint) in the CALIPSO telescope. PARASOL and Aura round off the A-train formation.

2.1 The Radar Model

Due to the non-negligible atmospheric attenuation by water vapor along the two-way beam path (e.g., from sensor to cloud or rain structure and back), the radar equation must account for the path integrated attenuation (PIA):

$$Z_{\text{true}}(i) = Z(i) + \text{PIA}(i) \quad . \tag{1}$$

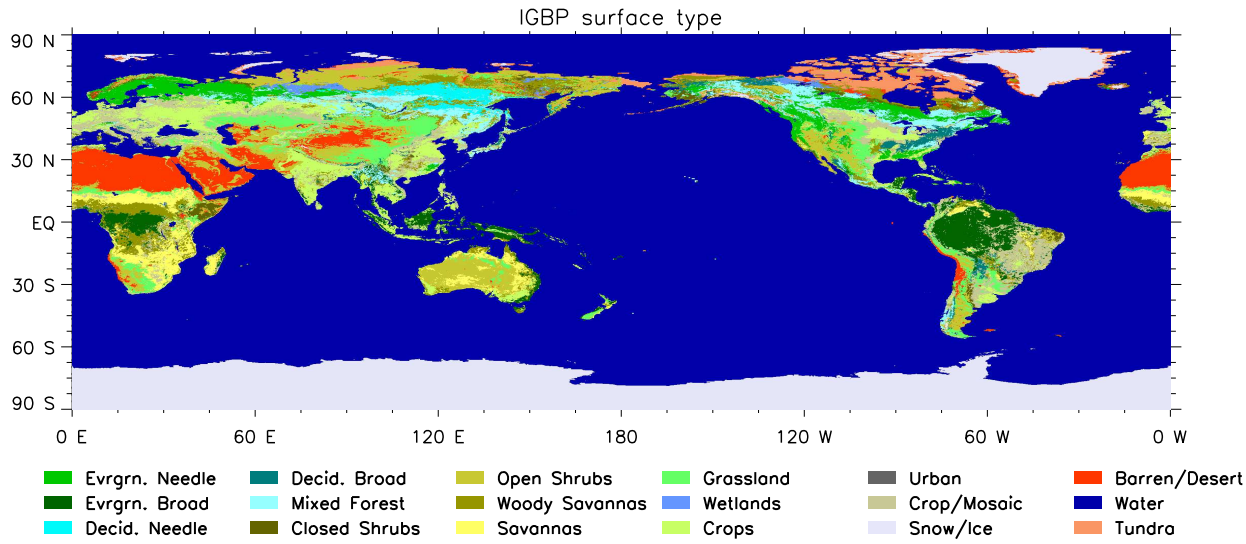

Figure 1: IGBP - type classification map.

Here Z_{true} and Z are the measured and the (true) radar reflectivities, while PIA is the 2-way attenuation term due to extinction by the atmospheric constituents and cloud particles. Index i indicated the gate being considered. The *forward model* is the mathematical description of the CPR, expressing the observed radar reflectivity Z as a function of the cloud/rain microphysical parameters. For example, we can assume that the cloud internal structure is characterized by a Marshall-Palmer (MP) distribution in the form (Liou, 1992):

$$n(D) = N_0 e^{-\Lambda D} \tag{2}$$

where D is the diameter of the cloud particles. Measurements (Liou, 1992) suggest a close empirical relationship between the slope factor Λ and the rainfall rate $\mathcal{R}$ of the form:

$$\Lambda = 41\mathrm{R}^{-0.21} \tag{3}$$

Using Mie scattering theory, based on the above distribution relationships, we precompute liquid/ice water content, rain rates, extinction coefficients, and corresponding radar reflectivities for ice and water cloud particles for a tabulated set of temperatures and effective particle diameters (characterizing the MP distribution). All results are stored in terms of look-up tables (LUTs) to be used by the operational retrieval scheme.

2.2 Retrieval Approach: The Optimal Estimation Technique

Since the radar extinction is due to both atmosphere and cloud effects, knowledge of the composition of the atmosphere and cloud is required. The superposition principle is used to separate these two components. Numerical model output, namely, the half-degree resolution Navy Operational Global Atmospheric Prediction System (NOGAPS), is used for constraining water vapor attenuation and for dictating which phase (liquid/ice) is to be used at each gate in the radar column. Using the previously mentioned LUTs, we further seek the appropriate cloud microphysical structure (i.e. its rain rates and/or liquid/ice water content) that best matches the observed reflectivity profile.

Due to the complexity of the forward model, for this retrieval process we choose the optimal estimation technique (e.g. Jazwinsky, 1970; Mitrescu et al., 2005) whereby the optimal environmental state vector minimizes a scalar cost function defined as a function of forward model sensitivity, background (first guess), retrieval constraints, and error covariances for these constituents. Details of the approach can be found in L'Ecuyer and Stephens, 2002. Our choice for this method is due also to its flexibility in allowing for additional physical constraints to the cost function construct. Here, we impose such a constraint in the form of a total column PIA, as estimated from the observed surface return. However, as discussed below, even the "well behaved" water surface serves up its own slew of caveats owing to sensitivity of the surface cross section to wind speed and sea surface temperature (SST).

2.3 Estimating the Path Integrated Attenuation (PIA)

Since attenuation affects all atmospheric radar volumes to greater or lesser extents, its specification is essential in retrieving accurate cloud parameters. This is particularly true for spaceborne estimates of surface rain, where the signal originating from most important radar gates (the near-surface gate itself) has been attenuated by the increasingly opaque atmosphere (over 1/2 of the atmosphere's water vapor resides in the lower troposphere at pressures exceeding 500 mb), clouds, and any rainfall above it. In other words, since our goal is to characterizing surface rainfall, we must have build a complete

account of the entire atmospheric/cloud vertical structure. Here, one can use the current observed surface return as indicator of the total PIA, provided that its equivalent clear-sky backscatter power is known. This is in principle possible, since we know the exact geo-location of the sub-satellite, and if we can further assume that the surface characteristics do not change significantly with time. Clearly these assumptions hold better for water than for land. In fact, radar returns from water surfaces are considered as good calibration references for many airborne and spaceborne microwave sensors (Menenghini et al., 2000; Li et al., 2005).

2.3.1 Reflectivity Model for the Surface Returns

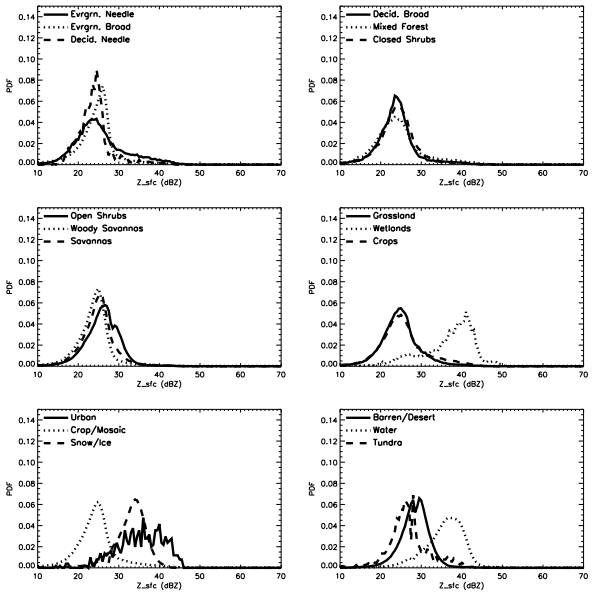

Figure 2: Surface Returns PDFs for various IGBP types. June 2 – July 7, 2006

Following this thought process, we constructed maps of mean surface returns using CloudSat surface returns in areas of clear sky (based on a statistical cloud mask run as a pre-processing step on all CPR data), thereby reducing PIA to only one contributor: the atmosphere. Although constructed using visible radiation, we use the IGBP surface classification (http://www-surf.larc.nasa.gov/surf/pages/IGBP list.html) for identifying specific land surface types (see figure 1). Further complicating the problem is the fact that CloudSat changed the alignment of its beam with respect to the local zenith three times (1.7 degrees forward, 0.0 degrees (nadir), and finally 0.16 degrees forward), with dramatically varying land surface returns resulting as a function of the high specular sensitivity. To illustrate this sensitivity we bin the measured data set into corresponding periods. Figures 2, 3, and 4 show the distribution of the surface returns (corrected for the atmospheric attenuation using NOGAPS) for all three viewing geometries used so far in the mission (http://cloudsat.cira.colostate.edu/).

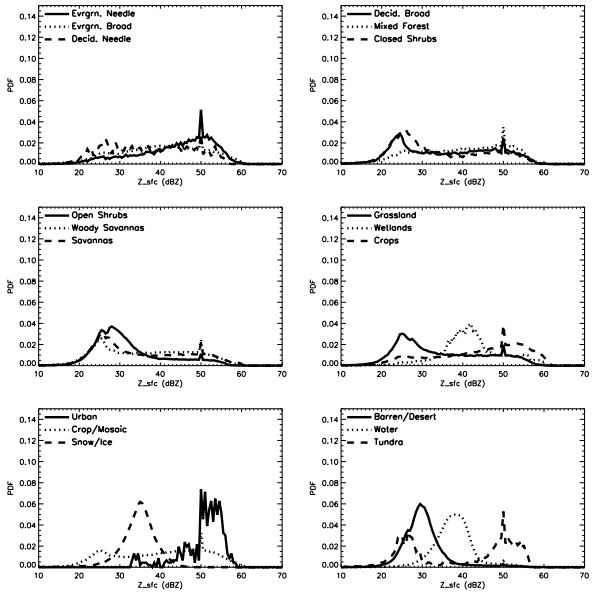

Figure 3: Surface Returns PDFs for various IGBP types. July 7 – August 15, 2006

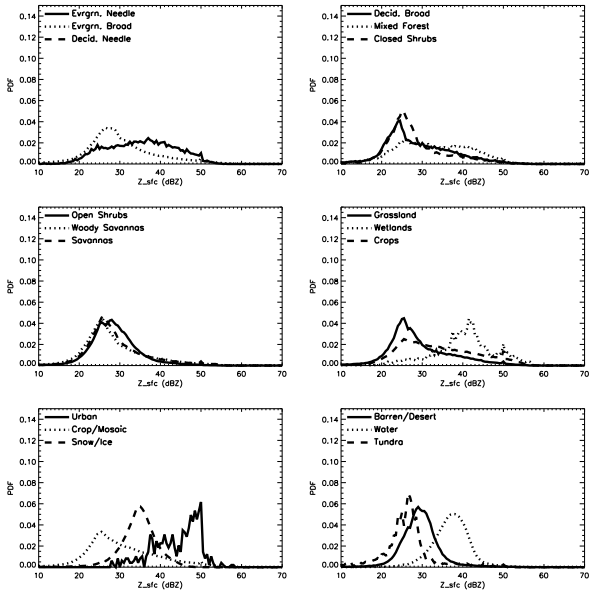

Figure 4: Surface Returns PDFs for various IGBP types. August 15 – Present, 2006

We note the large spread in signal for almost all the land types for the cases when specular reflection is the dominant regime (near-nadir) in contrast to the more diffuse return regime at larger incidence angles (julian days 153-188). However, over water these changes are not as pronounced. For simplicity at this stage in the research, we will limit our discussion attention on over-ocean profiles. In addition, and as seen from figure 5, the Antarctic ice-sheet is clearly distinguished. We avoid these regions by imposing a +/- 60 degree latitude range for our work

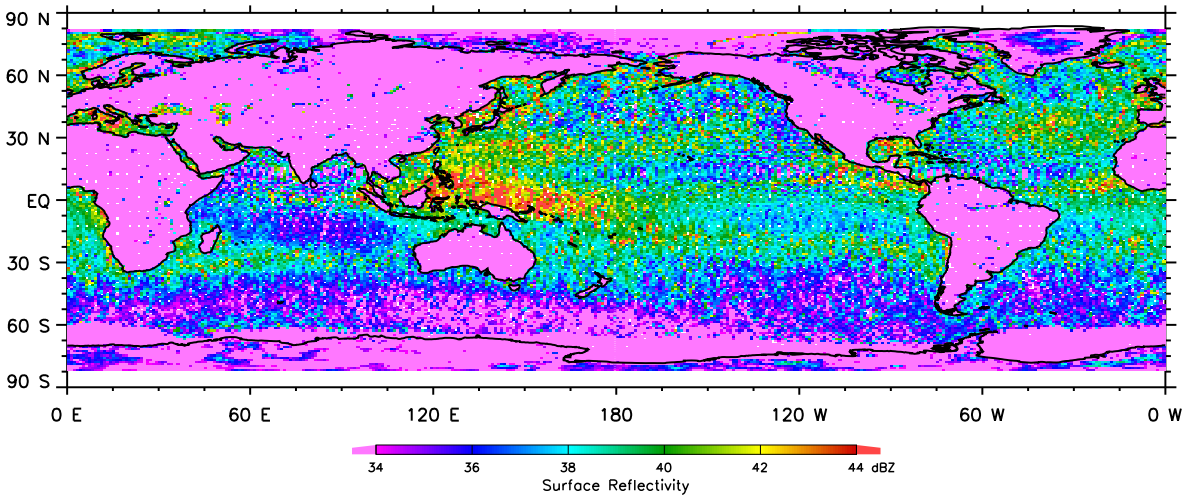

Figure 5: Surface Returns for IGBP types. June 2 – July 7, 2006.

region. As mentioned above, ocean surface was considered a good calibration media and many theoretical and experimental studies showed that this may be the case (Cox and Munk, 1954). We thus adopt the specular theory and come up with our own parameterization of the surface return in terms of the surface wind and temperature , also used to compute total-column atmospheric PIA. An example of such dependence with respect to wind speed – as modeled by NOGAPS (which assimilates SSM/I retrieved wind fields), is shown in figure 7, where the solid line shows our parameterization. Since the surface return also depends on SST via the complex index of refraction (i.e. Fresnel coefficient), we used the LUT tables to infer the corresponding adjustment. The final results of such a wind speed and SST correction are shown in figure 8 for each of the lat/lon boxes. At this time, the SST correction is based on a near surface air temperature, which may in some cases depart significantly from the true SST. In reprocessing exercises we will adjust these results to the NOGAPS skin temperature fields, and also examine the use of Aqua/AMSR-E retrievals of wind speed and SST as direct measurements for this purpose. It is likely that other unknown factors beyond SST and are responsible for the spread of the calculated surface reflectivities. The same pattern is visible in figure 6, which is simply the cumulative frequency distribution of the above results. However, we note that the current adjustment do have considerable information content, since the width of the distribution shrinks (solid-line=no correction; dashed line = wind and SST correction).

3. APPLICATION TO CLOUDSAT DATA

The CloudSat light rain retrieval is implemented on the Naval Research Laboratory's automated processing system (APS). CPR level-1B (radar return power, with calibration coefficients supplied) are obtained in near real-time (5-9 hr latency) thanks to coordination with the CloudSat Data Processing Center (DPC) located at the Cooperative Institute for Research of the Atmosphere (CIRA), co-located with Colorado State University (CSU) in Ft. Collins, CO.

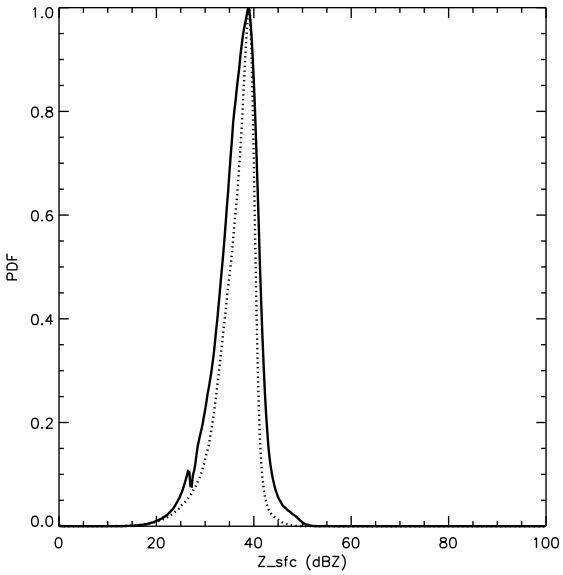

Figure 6: PDFs of Surface Reflectivity – solid line; with Wind and Temperature correction - dash line . June 2 - July 7, 2006

The rapid turn-around of these "first-look" files enables the operational community to utilize and gauge the operational viability of these novel data. Processing is delegated to an isolated high speed dual-node linux processor, which through an assortment of Perl and IDL procedures coordinates the end-to-end execution of cloud masking, rainfall retrieval, database pop-

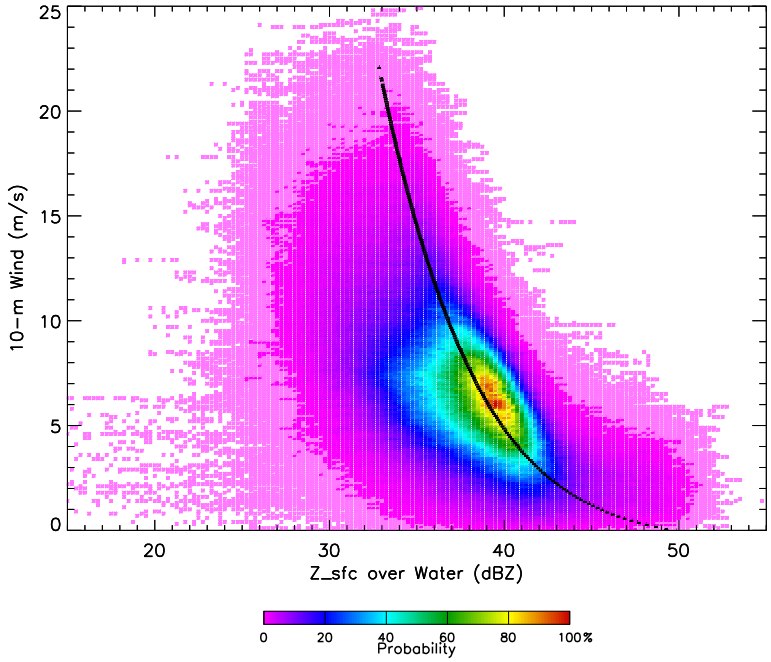

Figure 7: Surface Returns vs. Surface Wind Speed. June 2 – July 7, 2006.

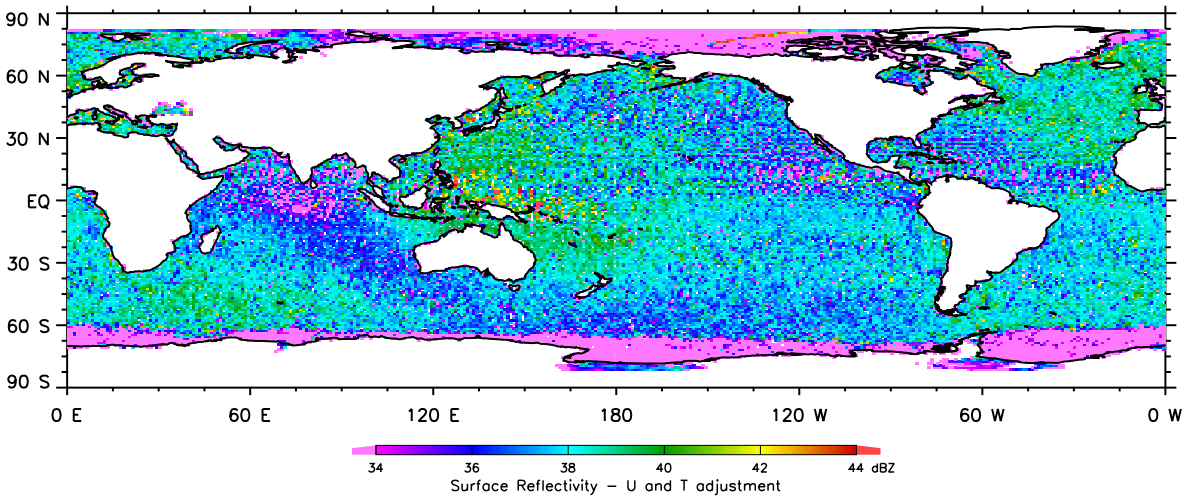

Figure 8: Wind and Temperature Corrected Surface Returns for IGBP types. June 2 – July 7, 2006.

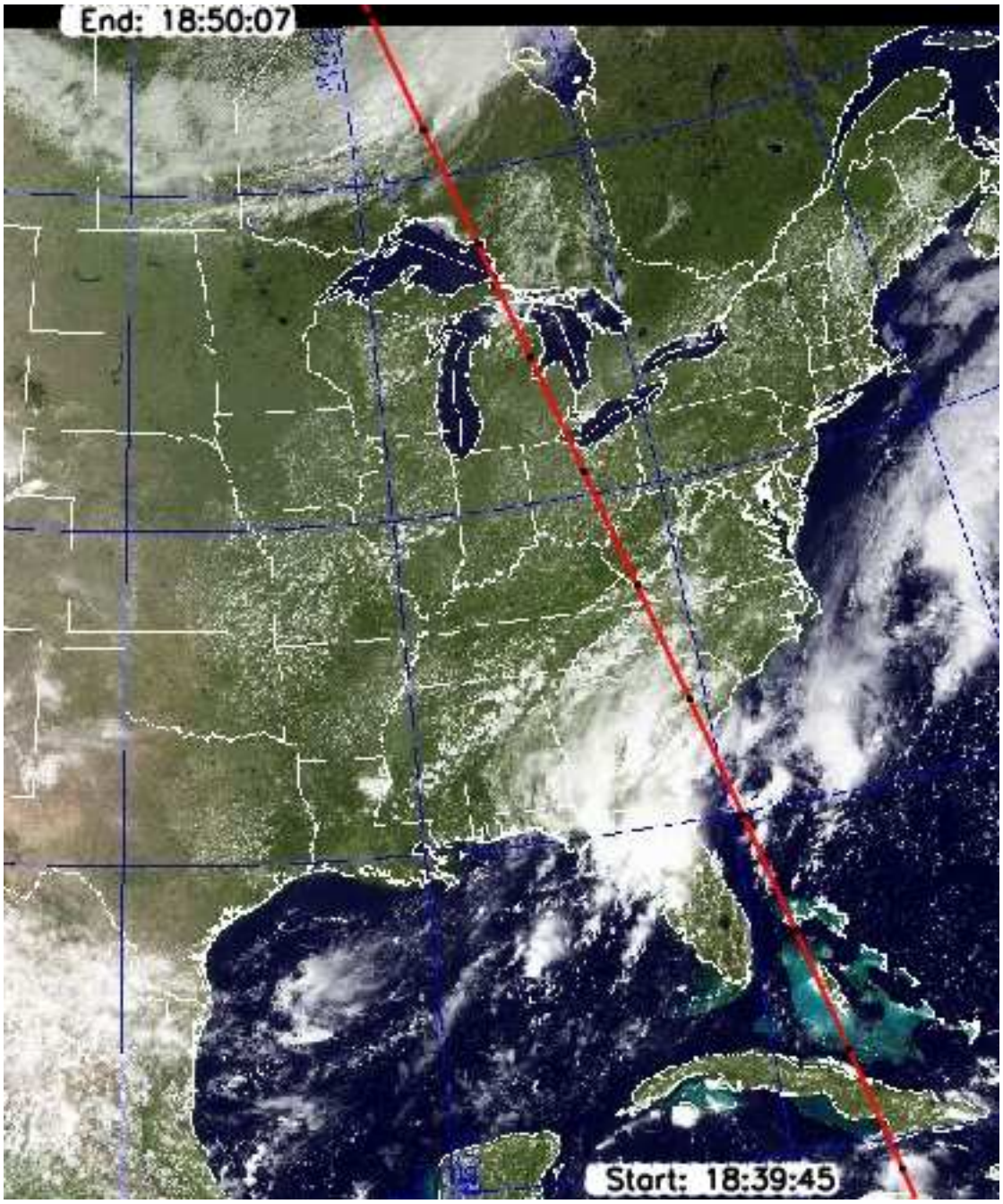

Figure 9: GOES-12 overview on 09/07/2006 18:30 UTC.

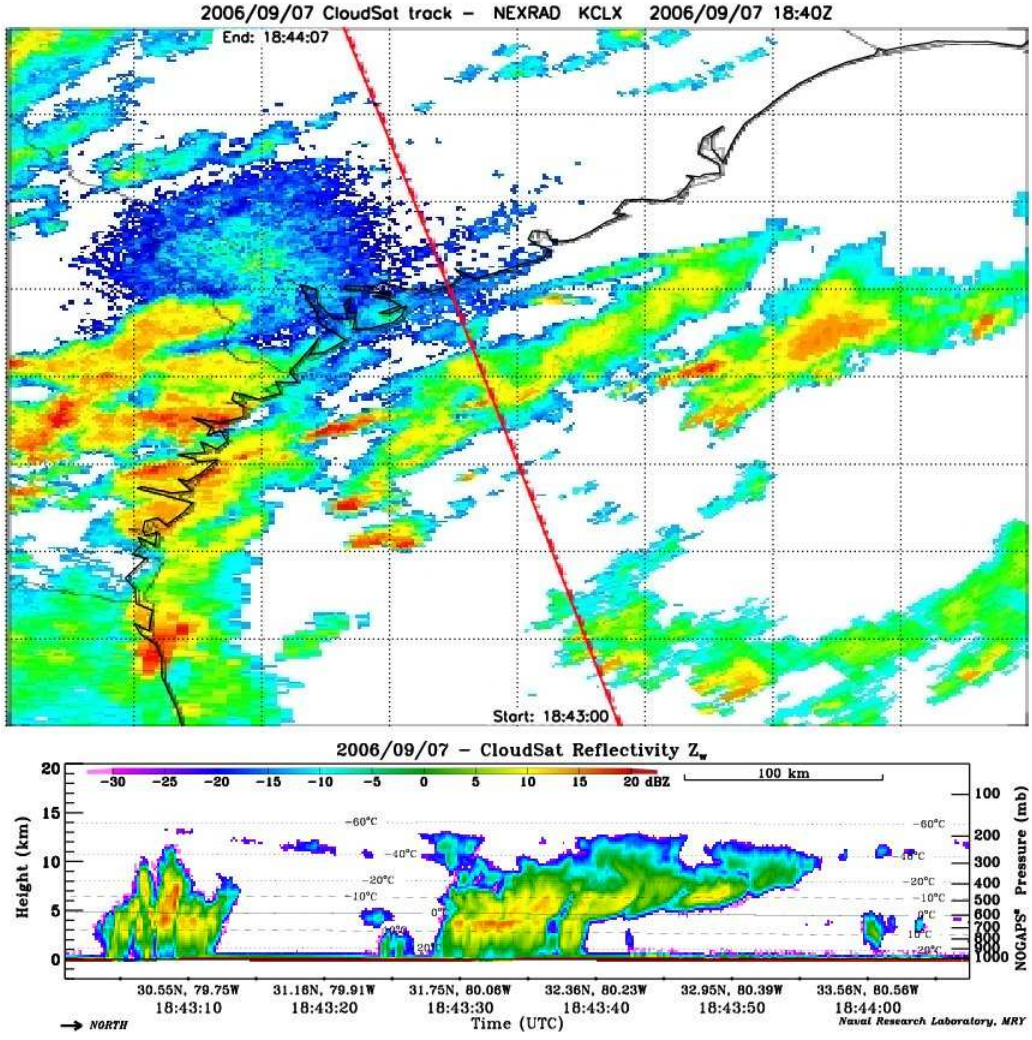

Figure 10: KCLX and CloudSat reflectivities.

ulation, and quick-look imagery rendering. Data are packaged within the original HDF data sets (along with other ancillary data and quality control flags) and archived locally as a CloudSat experimental product. Imagery are hosted in near real time on web pages support the DoD (e.g., Satellite Focus; Miller et al., 2006a), the tropical cyclone community (TC Web Page; www.nrlmry.navy.mil/tc pages/tc home.html; Hawkins et al., 2001), the general research/operational/public at large (NexSat; www.nrlmry.navy.mil/NEXSAT.html; Miller et al., 2006b). Currently, only CPR calibrated radar reflectivity data are posted to these sites, although several additions to the CloudSat product suite will be added in the near future.

3.1 Case Study - September 07 2006

We tested our reflectivity models (both cloud and surface) on a segment of CPR granule number 01928 (September 07 2006, around 18:40 UTC) corresponding to a pass over Hurricane Ernesto near North Carolina coast when it was in partial view of the Charleston, KCLX surface (WSR-88D "NEXRAD") radar. Figure 9 shows the corresponding GOES image with the CloudSat ground track superimposed. NOGAPS temperature (contours) and pressure (right ordinate axis) are also displayed. As a first-order validation of our light rain retrieval, we compared our CPR-retrieved precipitation rates for against those deduced form the KCLX radar (figure 10). The results shown in Figure 11 fare surprisingly well in light of the many problems associated with beam-filling, space/time mismatches, and differences in retrieval techniques: the rain rates retrieved using CloudSat data (solid line) are seen to be within reasonable limits of those inferred from the ground radar using known (i.e. calibrated) Z-R relationships (all other lines). Also apparent is the effect of the CPR footprint against the superior resolution of the ground radars.

3.2 (Very Preliminary) Global-Coverage Rain Rates Results

Applying our retrieval to the period June 2 - July 7 (Julian days 153 - 188), we calculated the mean precipitation rates for each pass over the ocean surfaces confined to the +/- 60 degree zonal belt (for reasons explained previously). Since the A-train is in a sun-synchronous orbit (1330 local time, ascending node), with a repeat period of approximately 16 days, it is understandable that cloud detection, hence precipitation estimates are biased by this non-uniform diurnal sampling. In other words, there is a possibility that a certain class of clouds within a particular regime may rain just hours before CloudSat passes over, and hence never be classified as precipitating, and vice versa (this was the primary reason for placement of TRMM in an asynchronous orbit). Only the "white noise" precipitation regimes will produce a statistically correct signal in our analysis. Moreover, due to the enhanced ground clutter that is present in the CloudSat signal (e.g., due to side-lobe contamination), we are compelled at this early stage in data processing to consider only radar returns from gate 5 (1.25 km) and up above the surface for characterizing surface rainfall. Thus, many shallow, low level clouds (predominantly marine stratocumulus systems) were excluded from these statistics.

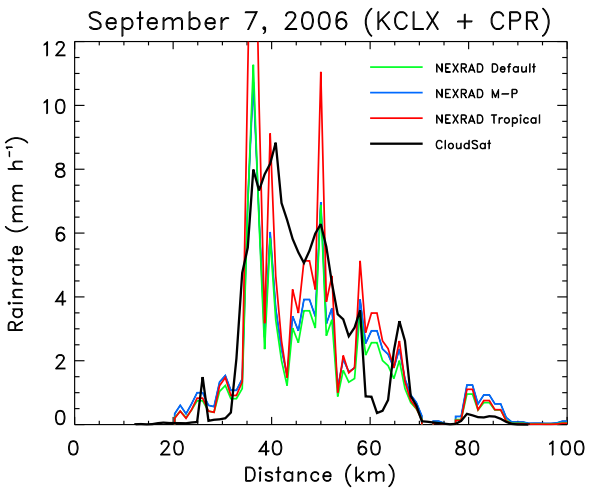

Figure 11: KCLX and CloudSat Rain Rates Comparison.

The above limitation in boundary-layer cloud/drizzle detection can also be inferred from figure 12, which shows precipitating cloud frequency. Here, known regions of stratocumulus clouds, some non-negligible fraction of which are presumably drizzling, are not "seen" by CloudSat. This is a problem that is currently being investigated by the CloudSat Science team. However, the winter storm track in the Southern Hemisphere (SH) is clearly visible, as well as the Inter-Tropical Convergence Zone (ITCZ) and other active convective regions. For the cases when precipitation was detected, the mean values were evaluated as shown in figure 13. Clearly the ITCZ, SH winter storms, and the Indonesian region display the most of the precipitation as expected, while the rest of the areas, while significant in size, have a small but non-negligible amount. This is also evident from the rain rates standard deviation map that supports the temporal- and spatial quasi-homogeneity of the light precipitating cloud systems (see figure 14). These light precipitating cloud regimes represent the heretofore unresolved closure of the Earth's water cycle, therefore representing a key element to energy balance. They are the ultimate target of this research effort.

4. SUMMARY AND FUTURE WORK

The present work explores the feasibility of using 94-GHz space borne radar data for detecting and quantifying light and perhaps even moderate rain rates. Examination of the CloudSat data even at these very early stages reveals promising results that lend hope to the notion that a very important component of the Earth's hydrology can

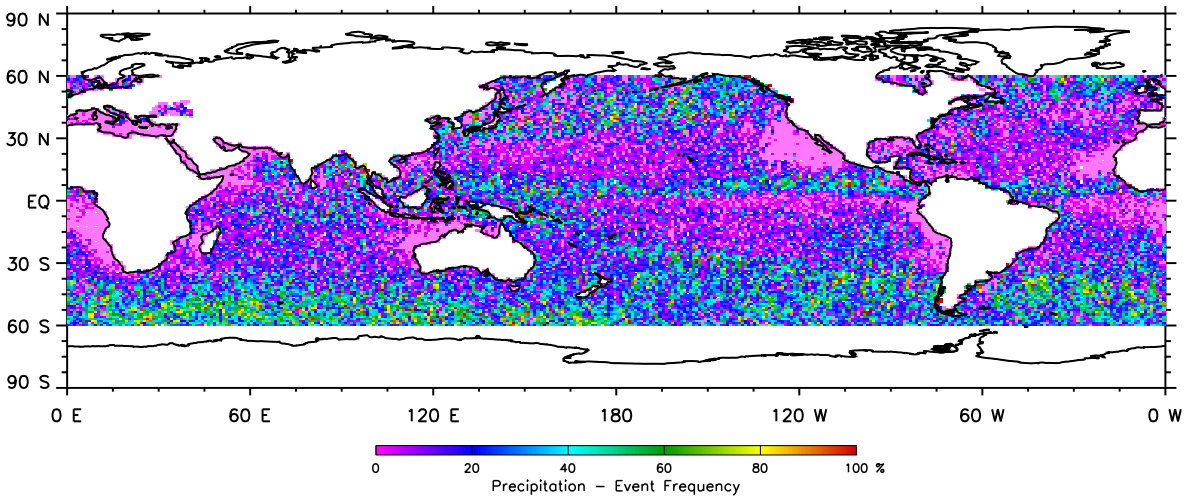

Figure 12: CloudSat Derived Precipitation Probability. June 2 – July 7, 2006.

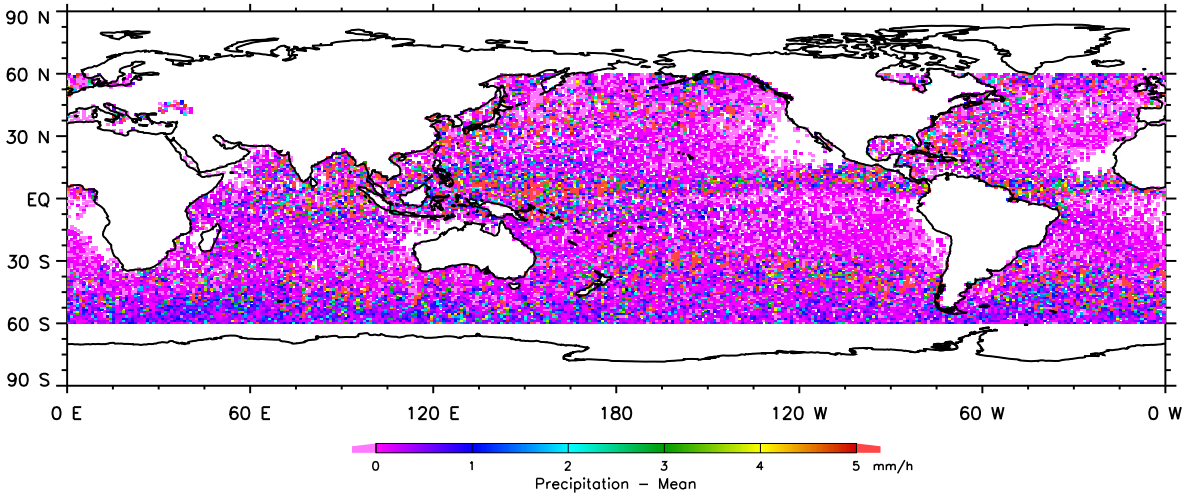

Figure 13: CloudSat Retrieved Mean Precipitation Rates. June 2 – July 7, 2006.

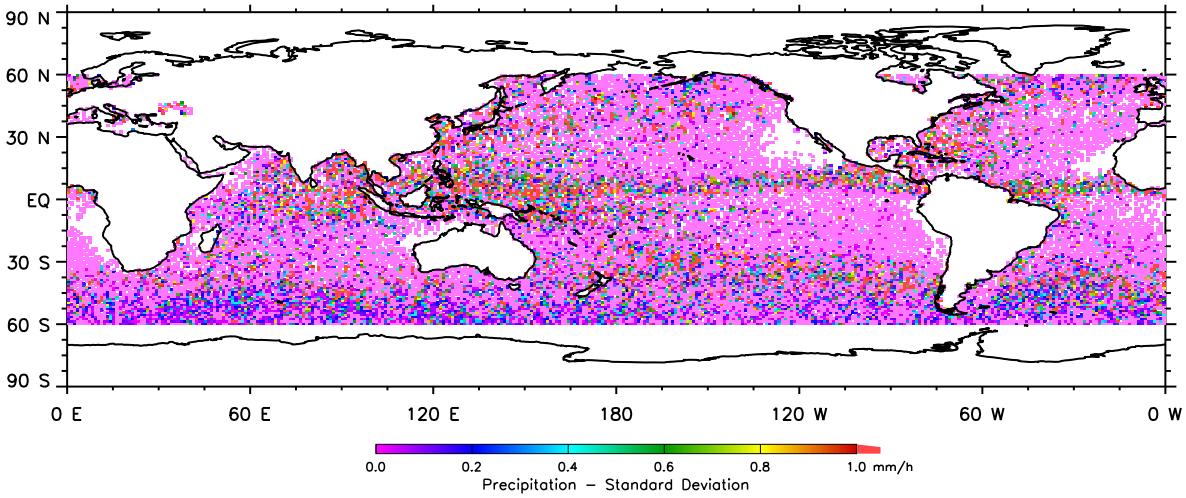

Figure 14: CloudSat Retrieved Standard Deviation of Precipitation Rates. June 2 – July 7, 2006.

be at last be measured on the global scale. Future work must expand the use of a modeled surface return to land surfaces, while improving the current model of water surface reflectivity return. Also, due in part to the large size of the sampled volume by the CPR sensor compared to the ground radars, the effect of multiply-scattered (MS) radiation must be taken into account (particularly in moderate rain regimes) either in terms of a filter or an account made in the forward model based, e.g., on Monte Carlo simulations.. Unfortunately, the MS effect is most pronounced at the furthest range gates where surface rain rates are being evaluated, and increases dramatically with the amount of cloud/rain water mass residing in the column above.

5. ACKNOWLEDGMENTS

The support of our research sponsors, the Oceanographer of the Navy through Program Office PEO-C4I and Space PMW-180 under Program Element PE-0603207N and the Office of Naval Research under Program Element PE-0602435N, is gratefully acknowledged.

6. REFERENCES

[1] Hawkins, J. D., T. F. Lee, K. Richardson, C. Sampson, F. J. Turk, and J. E. Kent, 2001: Satellite multisensor tropical cyclone structure monitoring, *Bull. Amer. Meteor. Soc.,* **82***,* 567-578.

[2] Held, I. M. and B. J. Soden, 2000: Water vapor feedback and global warming, *Annu. Rev. Energy Environ.,* **25***,* 441-475.

[3] Jazwinsky, A. H., 1970: *Stochastic Processes and Filtering Theory*, Academic Press, 376 pp.

[4] L'Ecuyer, T. S., and G. L. Stephens, 2002: An estimation-based precipitation retrieval algorithm for attenuating radars, *J. Appl. Meteo.,* **41***,* 272-285.

[5] Li, L., G. M. Heymsfield, L. Tian and P. E. Racette, 2005: Measurements of Ocean Surface Backscattering Using an Airborne 94-GHz Cloud Radar – Implication for Calibration of Airborne and Spaceborne W-Band Radars, *J. Atmos. Oceanic Techn.,* **22***,* 1033-1045.

[6] Liou, K. N., 1992: *Radiation and Cloud Processes in the Atmosphere*, Oxford University Press, 487 pp.

[7] Menenghini, R., T. Iguchi, T. Kozu, L. Liao, K.'I. Okamoto, J. .A. Johnes and J. Kwiatkowski, 2000: Use of the Surface Reference Technique for Path Attenuation Estimates From The TRMM Precipitation Radar, *J. A. M.,* **39***,* 2053-2070

[8] Miller, S. D., et al., 2006: MODIS Provides a Satellite Focus on Operation Iraqi Freedom, *Int. J. Rem. Sensing,* **27***,* 1285-1296.

[9] Miller, S. D., et al., 2006: NexSat: Previewing NPOESS/VIIRS Imagery Capabilities, *Bull. Amer. Meteor. Soc.,* **87***,* 433-446.

[10] Mitrescu, C., J. M. Haynes, G. L. Stephens, S. D. Miller, G. M. Heymsfield and M. J. McGill, 2005: Cirrus Cloud Optical, Microphysical and Radiative Properties Observed During CRYSTAL-FACE Experiment: A Lidar-Radar Retrieval System, *J. Geophys. Res.,* **110***,* doi:10.1029/2004JD005605.

[11] Stephens, G. L. et al., 2002: The CloudSat Mission and the A-Train: A New Dimension of Space-Based Observations of Clouds and Precipitation, *Bull. Amer. Meteorol. Soc.,* **12** 1771-1790.